Research Article GU J Sci 36(3): 1217-1229 (2023) DOI: 10.35378/gujs.987303

Gazi University

Journal of Science

http://dergipark.gov.tr/gujs

Rotor Field-Oriented Control of Doubly Fed Induction Generator in Wind Energy Conversion System

Zeki OMAC[1, *], Irfan ERDEM[2]

[1] *Department of Electrical and Electronics Engineering, Faculty of Engineering, Munzur University, 62000, Tunceli, Turkey*
[2] *Electronics Technology, Vocational School, Halic University, 34060 İstanbul, Turkey*

Highlights

•A 2 MW doubly fed induction generator (DFIG) is modeled for wind energy conversion systems.
•A robust rotor field-oriented control was developed to control the rotor side converter of the DFIG.
•A DFIG-based wind energy conversion system was experimentally tested.

Article Info

Received: 26 Aug 2021
Accepted: 17 Aug 2022

Keywords

Doubly Fed Induction Generator Wind Energy Rotor Field Oriented Control

Abstract

In this study, robust and high-performance vector control of a rotor side converter (RSC) was performed for stability and efficient operation doubly fed induction generator (DFIG) based on the variable speed wind turbine (VSWT). The mathematical model of the DFIG is simulated in the computer. Amplitude and frequency of the voltage in the DFIG were controlled for different values of load and variable speeds. In the experimental study, a DFIG-based wind turbine system was set up in the laboratory. The field position of the stator was detected from stator voltages by a phase-locked loop (PLL) circuit. The rotor position was measured with an incremental encoder connected to the rotor shaft of the DFIG. The angular position of the slip was calculated by the difference between the rotor and the stator field positions. The frequency and amplitude of rotor currents were determined with the angular position of slip. To generate output voltages of converter feeding rotor windings, the space vector pulse width modulation (SVPWM) technique was used. In the experimental study, the RSC was controlled with the DS1103 board. The prepared experiment set was tested at different operating speeds.

1. INTRODUCTION

Efforts to meet the world's rising energy demand from renewable energy sources including wind energy have increased because they are clean, economical, and reliable. Wind energy has the highest growth rate in electricity generation from renewable energy sources [1-3]. The kinetic energy of the wind is converted to electrical energy by using wind turbines. The variable speed wind turbine is a turbine designed to provide maximum energy efficiency at various wind speeds. The DFIG is the most common generator used for generating electrical energy in the variable speed wind turbine [4-8].

The DFIG has been used in half of the wind energy market due to its benefits such as high efficiency, low cost, and unique structure [8]. Also, the active and reactive power in the DFIG can be separately controlled [9-14]. In addition, the power loss of the DFIG is lower than that of squirrel cage induction generator (SCIG) and permanent magnet synchronous generator (PMSG). Furthermore, it has a greater power quality since the stator winding is directly connected to the grid without the need for a power converter. It does not contain any rare elements, such as magnets. Moreover, rotor side converter (RSC) power is 30% of nominal power of the DFIG [15-19]. This allows the control of the rotor side with the lower power RSC of the DFIG while the PMSG and SCIG need more power. Thus, the cost of the wind turbine system is greatly reduced. Furthermore, it is robust and stable in face of external disturbances [20-26].
The stability of voltage and frequency is an important issue in the generation of electrical energy from wind turbine systems with DFIG. In [5], the reactive power of the generator is controlled in a simulation model

*Corresponding author, e-mail: zomac@munzur.edu.tr

by controlling the rotor voltage for the stability of the output voltage of the generator at different speeds. But they did not prove their results in the experiment. In addition, harmonic currents induced by non-linear loads are filtered from the grid and active and reactive powers are regulated [9]. Active and reactive powers are controlled with the developed optimal controller of rotor currents [24].

The design of the DFIG controller has been made for stable operation in weak grids [11]. DFIG-fed grids, the stator harmonic currents are suppressed by the feedforward regulator. In addition, the stator harmonic voltages are compensated by rotor harmonic voltages [12]. In an autonomous grid, DFIG and solar energy are used together in the generation of electrical energy [14]. The model reference adaptive system was used to predict rotor position and speed. A wind-diesel hybrid system with a battery energy storage system in a microgrid was presented by Tiwari [15]. In a study [16], the DFIG system impedance considering the phase-locked loop (PLL) was examined. The resonance potential caused by the PLL has been identified. An improved direct power control strategy without PLL was investigated for DFIG under unbalanced and distorted voltage conditions [19].

A new control strategy has been developed to increase the primary frequency and reduce low-frequency oscillations in DFIG using the RSC [6]. DFIG frequency control is used in wind farms [10]. Commercial converters have been used for RSC and GSC in DFIG stator flux-oriented control [17]. The frequency is controlled in DFIG by using a virtual synchronous generator control strategy for the RSC converter and an inertial synchronization control strategy for the GSC converter [18]. Model predictive control [3], optimal efficiency control [4], reduced order state observer feedback control [7], and finite control set model predictive control [21] are applied for DFIG control. It investigated the optimal power converter selection in a DFIG wind turbine system for enhanced system-level reliability [20]. Predictive torque control is used to provide less torque ripple and minimization losses in the DFIG-DC system [22]. Multivariable state feedback current controllers are proposed for GSC and RSC [8]. An adaptive controller based robust speed estimation technique is used for the position sensorless control of DFIG [1]. Rotor speed is estimated by using stator and rotor currents. The position sensorless control of the brushless DFIG is provided by using the control winding current by a model reference adaptive system (MRAS) observer [23]. The authors found that the MRAS observer was constant and had a good dynamic performance while being robust to uncertainties in parameter variations.

The voltage and frequency stability are the most important factors in DFIG that there are negatively affected by the variation in the turbine speed depending on the wind speed. In the present study, a model of a wind turbine DFIG system is simulated in a computer for voltage and frequency stability. The RSC has been used to control the DFIG which is under variable speeds. Thus, the simulation results are obtained. An experimental setup of DFIG is prepared in a laboratory to validate the simulation results. This paper is arranged as follows. The dynamic mathematical model of the DFIG is constructed in section 2. Then, the vector control of the rotor side controller is detailed in section 3. Following that, simulation and experimental results are presented in section 4 and, conclusions are given in section 5.

2. DYNAMIC MATHEMATICAL MODEL OF DFIG

There are three-phase windings in the rotor of doubly fed induction machines (DFIM) as well as in the stator. In this regard, energy input and output may be made from both the rotor and stator sides of these machines. The grid is not only connected to the stator windings but also connected to the rotor windings by a back-to-back converter through the brush ring system. The torque, speed and power factors in the DFIG are all controlled by RSC. The constant DC bus voltage is controlled by the GSC in the back-to-back converter. Double-sided energy input and output are provided from the grid depending on the rotor power. The rotor winding consumes energy from the grids at sub-synchronous speeds. If the rotor of DFIG rotates faster than the synchronous speed, it will feed to the grid.

It is assumed that the flux is sinusoidal in the air gap and the stator windings are spread arrangement around the stator in the dynamic mathematical model of DFIG. The magnetic permeability of iron sheets is taken infinite and iron losses are neglected. It is accepted that the resistance and inductance do not change with

temperature and frequency. In Figure 1, the equivalent circuit of DFIG is given on the d-q reference axis rotating at the synchronous speed.

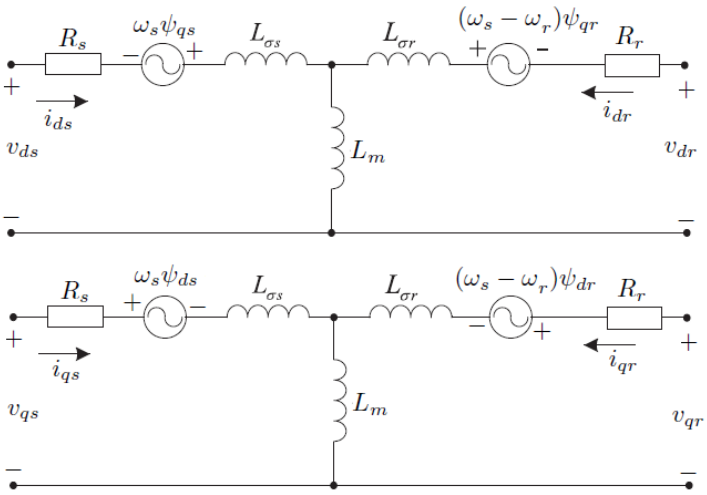

Figure 1. *Equivalent circuit of the DFIG in synchronously rotating d-q frame*

Equations of (1) - (4) can be written for stator and rotor voltages from the DFIG equivalent circuit [7-9]

$$v_{ds} = R_s i_{ds} + L_s \frac{di_{ds}}{dt} - \omega_s \psi_{qs} + L_m \frac{di_{dr}}{dt}, \tag{1}$$

$$v_{qs} = R_s i_{qs} + L_s \frac{di_{qs}}{dt} + \omega_s \psi_{ds} + L_m \frac{di_{qr}}{dt}, \tag{2}$$

$$v_{dr} = R_r i_{dr} + L_r \frac{di_{dr}}{dt} - (\omega_s - \omega_r)\psi_{qr} + L_m \frac{di_{ds}}{dt}, \tag{3}$$

$$v_{qr} = R_r i_{qr} + L_r \frac{di_{qr}}{dt} + (\omega_s - \omega_r)\psi_{dr} + L_m \frac{di_{qs}}{dt}, \tag{4}$$

where v_{ds}, v_{qs} represent the stator d-q axis voltages; v_{dr}, v_{qr} are the rotor d-q axis voltages; i_{ds}, i_{qs} are the stator d-q axis currents; i_{dr}, i_{qr} are the rotor d-q axis currents; $L_{\sigma s}, L_{\sigma r}$ represent the stator and rotor leakage inductance; L_m is the magnetizing inductance; R_s is the stator resistance; R_r is the rotor resistance; ω_s, ω_r are the stator flux synchronous angular speed and rotor flux angular speed; and $\psi_{ds}, \psi_{qs}, \psi_{dr}, \psi_{qr}$ represent the stator and rotor d-q axis flux linkages, respectively.

The stator flux linkages and rotor flux linkages may be indicated regarding self-inductances by Equations (5) - (8)

$$\psi_{ds} = L_s i_{ds} + L_m i_{dr}, \tag{5}$$

$$\psi_{qs} = L_s i_{qs} + L_m i_{qr}, \tag{6}$$

$$\psi_{dr} = L_r i_{dr} + L_m i_{ds}, \tag{7}$$

$$\psi_{qr} = L_r i_{qr} + L_m i_{qs}. \tag{8}$$

The stator (L_s) and rotor (L_r) self-inductances can be defined as sum of the magnetizing inductance and the stator and rotor leakage inductances in Equations (9) - (10)

$$L_s = L_m + L_{\sigma s}, \tag{9}$$

$$L_r = L_m + L_{\sigma r}. \tag{10}$$

The mechanical dynamics of the system can be written for DFIG as in Equations (11)

$$\frac{d\omega_m}{dt} = \frac{1}{J}(T_m - T_e - B\omega_m) \tag{11}$$

where ω_m, J, T_m, T_e and B represent the rotor mechanical angular speed, the moment of inertia, the mechanical torque in the shaft, electromagnetic torque, and the coefficient of viscous friction, respectively.

The relation between rotor mechanical angular speed ω_m and rotor field angular speed ω_r is given in Equation (12)

$$\omega_r = \omega_s - p\omega_m \tag{12}$$

where p represents the number of pole pairs of the DFIG. The electromagnetic torque and the total stator active and reactive power can be computed from stator and rotor currents and voltages Equations (13) - (15)

$$T_e = \frac{3}{2}pL_m(i_{dr}i_{qs} - i_{qr}i_{ds}), \tag{13}$$

$$P_s = \frac{3}{2}(v_{ds}i_{ds} + v_{qs}i_{qs}), \tag{14}$$

$$Q_s = \frac{3}{2}(v_{qs}i_{ds} - v_{ds}i_{qs}). \tag{15}$$

DFIGs usually operate in the range of ± 30% the generator synchronous speed. The ability of the generator to be controlled within this range depends on the slip rate of the generator. In induction machines, the general slip expression (s) is given in Equation (16)

$$s = \frac{\omega_s - p\omega_m}{\omega_s} = \frac{\omega_r}{\omega_s}. \tag{16}$$

The slip expression can be defined as the ratio of the frequency of the rotor currents (f_r) to the frequency of the stator currents (f_s) in Equation (17)

$$s = \frac{f_r}{f_s}. \tag{17}$$

The stator field angular speed is constant. Therefore, the slip can be set according to the rotor field angular speed. The conversion of the mechanical power to electrical power in induction machines can be expressed by Equation (18)

$$P_m = P_s + P_r \tag{18}$$

where P_m, P_s and P_r represent the total mechanical power in the generator shaft, the electrical power received from the stator and the power received or delivered from the rotor, respectively. Turbine power is the sum of powers generated by the stator and rotor. The expression of power in terms of the torque equation is defined in Equations (19)

$$T_m\omega_s = T_m\omega_r - P_r \tag{19}$$

where T_m describes the mechanical torque of wind turbine. By rearranging the Equation (18), the rotor power (P_r) can be rewritten as shown in Equations (20)

$$P_r = -T_m(\omega_s - \omega_r). \tag{20}$$

Rotor power (P_r) and stator power (P_s) can be correlated as given in Equations (21)

$$P_r = -sT_m\omega_s = -P_s. \tag{21}$$

Active and reactive powers can be defined for rotor as shown in Equations (22) and (23)

$$P_r = \frac{3}{2}\left(v_{dr}i_{dr} + v_{qr}i_{qr}\right), \tag{22}$$

$$Q_r = \frac{3}{2}\left(v_{qr}i_{dr} - v_{dr}i_{qr}\right). \tag{23}$$

The block diagram of the DFIG wind turbine is given in Figure 2. The power is controlled on the stator and rotor sides by the GSC and RSC. The amplitude and frequency of the voltage applied to rotor winding are adjusted with the stator rotation field and rotor speeds. Thus, it is ensured that the DFIG generates voltage at a constant amplitude and frequency for grid, which is unaffected by turbine speed variations.

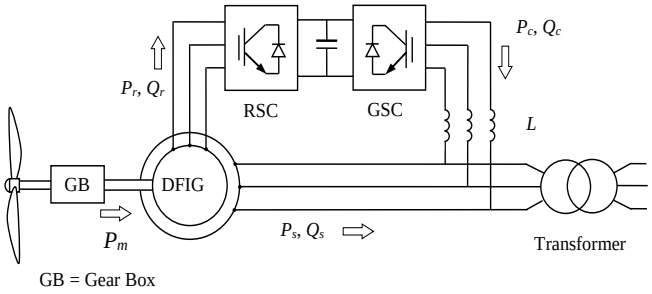

Figure 2. *Block diagram of a DFIG driven by wind turbine*

3. VECTOR CONTROL OF DFIG

Control of the DFIG includes two parts which are the control of RSC and GSC.

3.1. Control of RSC

There are different control methods for control of the RSC. Direct vector control is a basic method used to control the DFIG with the stator flux or the voltage reference. Furthermore, indirect vector control and direct torque control methods are used for controlling the RSC. The basis of the vector control method is the d-q axis transformations. The conversion of three-phase generator model variables to the direct quadrature (d-q) axis set, which is 90 degrees apart, is provided to be independently controlled. The DFIG is controlled as a separate direct current motor with the d-q axis conversions.

In orientated methods, the stator voltage is set to the d axis as seen in Figure 3 instead of the stator flux at a synchronously rotating d-q reference frame. Thus, rotor currents are controlled by providing $V_s = V_{sd}$ equation. If the stator resistance is disregarded in the calculation of stator flux, there will be a ninety-degree phase difference between the stator voltage and the flux. The voltage vector is shifted to ninety degrees by the park transformation. The block diagram of vector controlled DFIG is given in Figure 4. The stator rotating flux position is found in Equation (24)

$$\theta_s = arctan\frac{V_{s\beta}}{V_{s\alpha}}. \tag{24}$$

3.2. Phase Locked Loop

The control of renewable energy systems mainly depends on the phase, magnitude and frequency of the grid voltage and the synchronization algorithm that must be determined accurately. Phase-locked loop (PLL) techniques are used to determine the grid voltage phasor position. PLL methods are the most

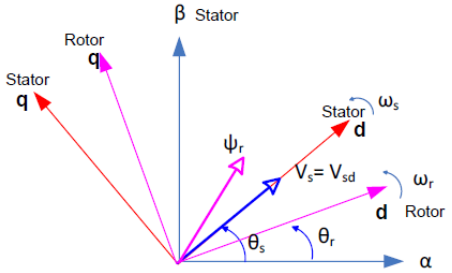

Figure 3. *Vector diagram of the stator and rotor fluxes*

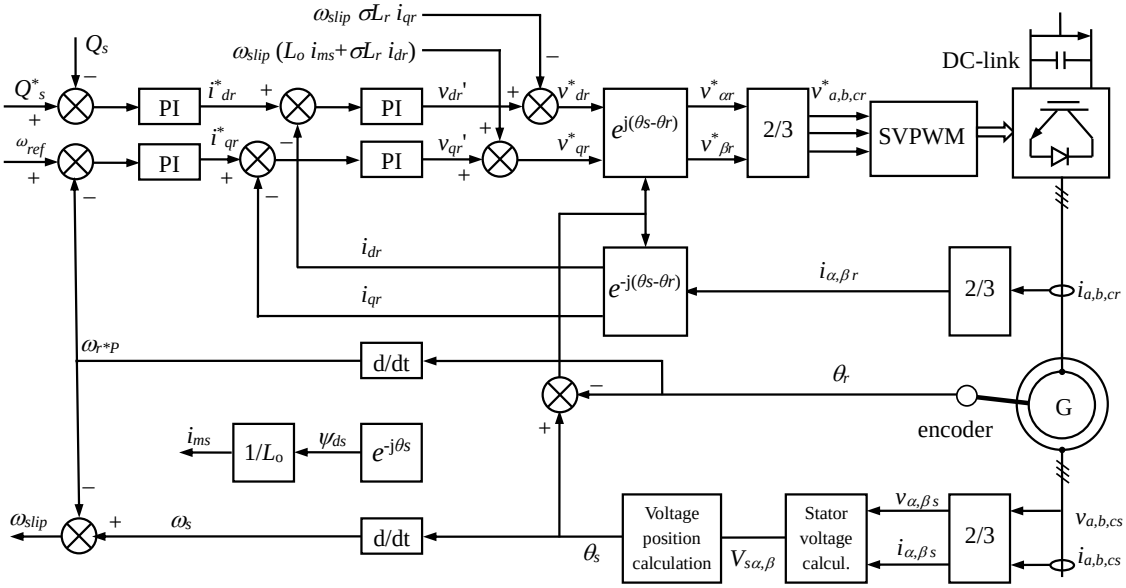

Figure 4. *Vector control block diagram of the DFIG*

frequently used method for calculating the voltage angle and frequency due to their simplicity, stability, and robustness to signal disturbances.

In the 3-PLL control, d-q axis voltages are obtained from three-phase abc voltages to d-q axis conversions in the synchronously rotating reference frame. If this voltage is set to the d axis, $V = V_d$ and $V_q = 0$ equation will be obtained. Then, the V_q is controlled with the proportional integral (PI) controller and the initial value, 2πf, is added to the controller output. As a result, the value of angular speed is obtained.

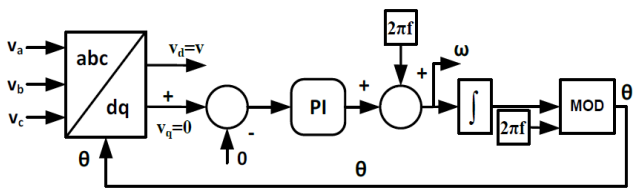

Figure 5. *Control scheme of the PLL*

The integration of angular speed gives the angle of position, whose information is sent to the abc-dq conversion. The control scheme of the PLL is shown in Figure 5.

3.3. Space Vector Pulse Width Modulation

Nowadays, one of the most popular techniques in the generation of pulse width modulation (PWM) has been the space vector pulse width modulation (SVPWM) technique. The SVPWM technique offers a higher voltage level and more efficient use of DC bus voltage than the sinusoidal PWM method. The minimum switching loss can be achieved by choosing the appropriate switching scheme. In the output current, the low harmonic is obtained by switching patterns. It also has the advantage of being able to practice at a lower switching frequency. The algorithm's complexity due to the increased number of levels in multi-level inverters can be expressed as the only disadvantage of this technique. Since the RSC generally operates at a low frequency, the generated signals are distorted at zero crossings. The SVPWM method has been found to minimize this problem experimentally. For this reason, the SVPWM method is applied in the RSC control.

3.4. SVPWM Algorithm

For generating the desired space vector, which the switches require a PWM signal, resulting voltage, to generate, the main vectors used in the present study are given in Table 1. Each combination of switches generating a space vector for the two-level inverter is presented in Figure 6. These space vectors have six different sectors formed by a combination of dual.

Of these vectors, V_0 and V_7 vectors generate zero output voltage. Therefore, these vectors are called zero vector. V_{ref} is obtained in Equation (25) after Clarke transformation from V_α and V_β. Then, the θ angle is calculated in Equations (26) for the region where the vector V_{ref} is located. After calculating the θ angle of the region, the sector in which the V_{ref} vector is located needs to be determined

$$V_{ref} = \sqrt{{V_\alpha}^2 + {V_\beta}^2}\,, \tag{25}$$

$$\theta = tan^{-1}\left(\frac{V_\beta}{V_\alpha}\right). \tag{26}$$

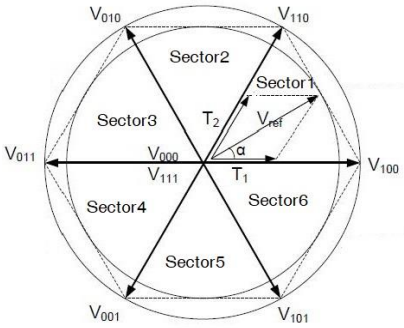

Figure 6. *Space vectors diagram for two level-inverter*

The matrix Equation (27) is used to transform the three-phase V_a, V_b, V_c phase voltages to two-phase V_α and V_β voltages

$$\begin{bmatrix} V_\alpha \\ V_\beta \\ V_o \end{bmatrix} = \frac{2}{3}\begin{bmatrix} 1 & -1/2 & -1/2 \\ 0 & \sqrt{3}/2 & -\sqrt{3}/2 \\ 0.5 & 0.5 & 0.5 \end{bmatrix}\begin{bmatrix} V_a \\ V_b \\ V_c \end{bmatrix}. \tag{27}$$

If the period of the applied PWM signal is T_s and the V_{ref} vector is assumed in sector 1, T_0, the time of vector V_0, T_1, the time of the V_1 vector, T_2, time of the vector V_2, are given in Equations (28) - (30)

$$\int_0^{T_s}\bar{V}_{ref}\,dt = \int_0^{T_1}\bar{V}_1\,dt + \int_{T_1}^{T_1+T_2}\bar{V}_2\,dt + \int_{T_1+T_2}^{T_s}\bar{V}_0\,dt, \tag{28}$$

$$T_s.\bar{V}_{ref} = (T_1.\bar{V}_1 + T_2.\bar{V}_2), \tag{29}$$

$$T_s.\left|\bar{V}_{ref}\right|.\begin{bmatrix}cos(\theta)\\ sin(\theta)\end{bmatrix} = T_1.\bar{V}_1.\begin{bmatrix}1\\0\end{bmatrix} + T_2.\bar{V}_2.\begin{bmatrix}cos(\pi/3)\\ sin(\pi/3)\end{bmatrix}. \tag{30}$$

T_1, T_2 and T_0 are generally calculated as in Equations (31) - (33) for all sectors, shown in Figure 7

$$T_1 = T_s.\frac{|\bar{V}_{ref}|}{V_{dc}}.\frac{sin(\pi/3-\theta)}{sin(\pi/3)}, \tag{31}$$

$$T_2 = T_s\frac{|\bar{V}_{ref}|}{V_{dc}}.\frac{sin(\theta)}{sin(\pi/3)}, \tag{32}$$

$$T_0 = T_s - (T_1 + T_2). \tag{33}$$

Table 1. *Switching conditions and combination of output voltages*

a	b	c	V_a	V_b	V_c	V_{ab}	V_{bc}	V_{ca}
0	0	0	0	0	0	0	0	0
1	0	0	$\frac{2}{3}V_{dc}$	$-\frac{1}{3}V_{dc}$	$-\frac{1}{3}V_{dc}$	1	0	-1
1	1	0	$\frac{1}{3}V_{dc}$	$\frac{1}{3}V_{dc}$	$-\frac{2}{3}V_{dc}$	0	1	-1
0	1	0	$-\frac{1}{3}V_{dc}$	$\frac{2}{3}V_{dc}$	$-\frac{1}{3}V_{dc}$	-1	1	0
0	1	1	$-\frac{2}{3}V_{dc}$	$\frac{1}{3}V_{dc}$	$\frac{1}{3}V_{dc}$	-1	0	1
0	0	1	$-\frac{1}{3}V_{dc}$	$-\frac{1}{3}V_{dc}$	$\frac{2}{3}V_{dc}$	0	-1	1
1	0	1	$\frac{1}{3}V_{dc}$	$-\frac{2}{3}V_{dc}$	$\frac{1}{3}V_{dc}$	1	-1	0
1	1	1	0	0	0	0	0	0

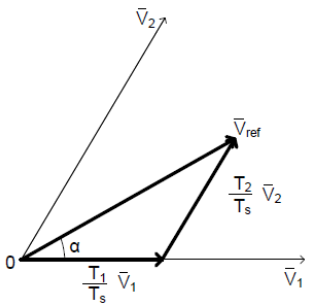

Figure 7. *θ angle, V_1, V_2 and V_{ref} vectors for a sector*

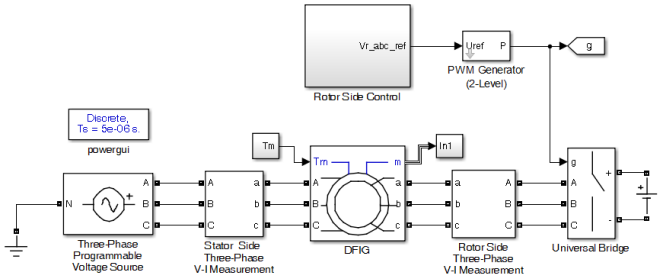

Figure 8. *Simulation model of a DFIG*

4. SIMULATION AND EXPERIMENTAL RESULTS

The mathematical model of a DFIG generating electricity from wind turbine is simulated in the computer. Simulation model of the DFIG is given in Figure 8. Amplitude and frequency of the voltage generated by DFIG at various wind speeds and under different loads are controlled by using the PI controller. In Table 2, simulation parameters are given for DFIG. The experimental set shown in Figure 9 is used to acquire the experimental results. In the experimental study, DFIG is rotated with a three-phase squirrel cage induction motor. In Table 3, the parameters of DFIG used in the experimental study are given. Phases currents and voltages are measured by LA -55P current sensors and LV-25P voltage sensors, respectively. The RSC of the DFIG is controlled with the DS1103 board. The measured current and voltage signals are transferred to the DS1103 control board using analog-digital converter inputs. The rotor speed of the DFIG is measured with an incremental encoder that generates 2500 pulses in per revolution. PWM signals of RSC switches are generated at a 5 kHz switching frequency.

In the simulation study, the speed and load torque of DFIG are initially set as 157.14 rad/s synchronous speed and 0 Nm load torque in the range of 0-0.4 seconds. Subsequently, the sub-synchronous speed of 141.426 rad/s and the load torque of 3000 Nm are made in the DFIG 0.4-2.6 second interval. Between 2.6-3.6 seconds, the up synchronous speed is 172.84 rad/s and the load torque is 6000 Nm. Simulation results are shown in Figure 10. During simulation, the rotor current d-axis component is taken to be zero (i_{rd} = 0 A).

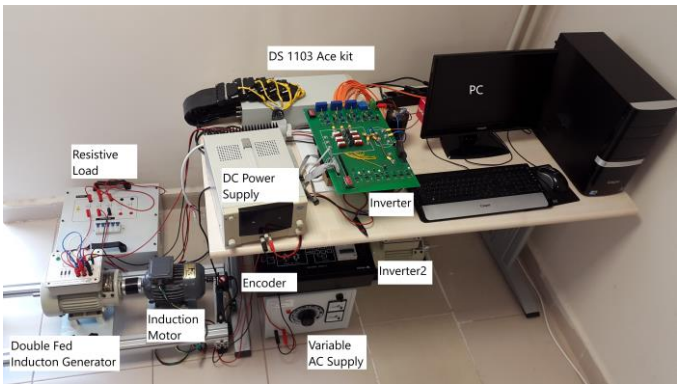

Figure 9. *Experimental test setup*

Experimental results are given for sub-synchronous speed (600 rpm) and for up synchronous speed (900 rpm) in Figure 11.

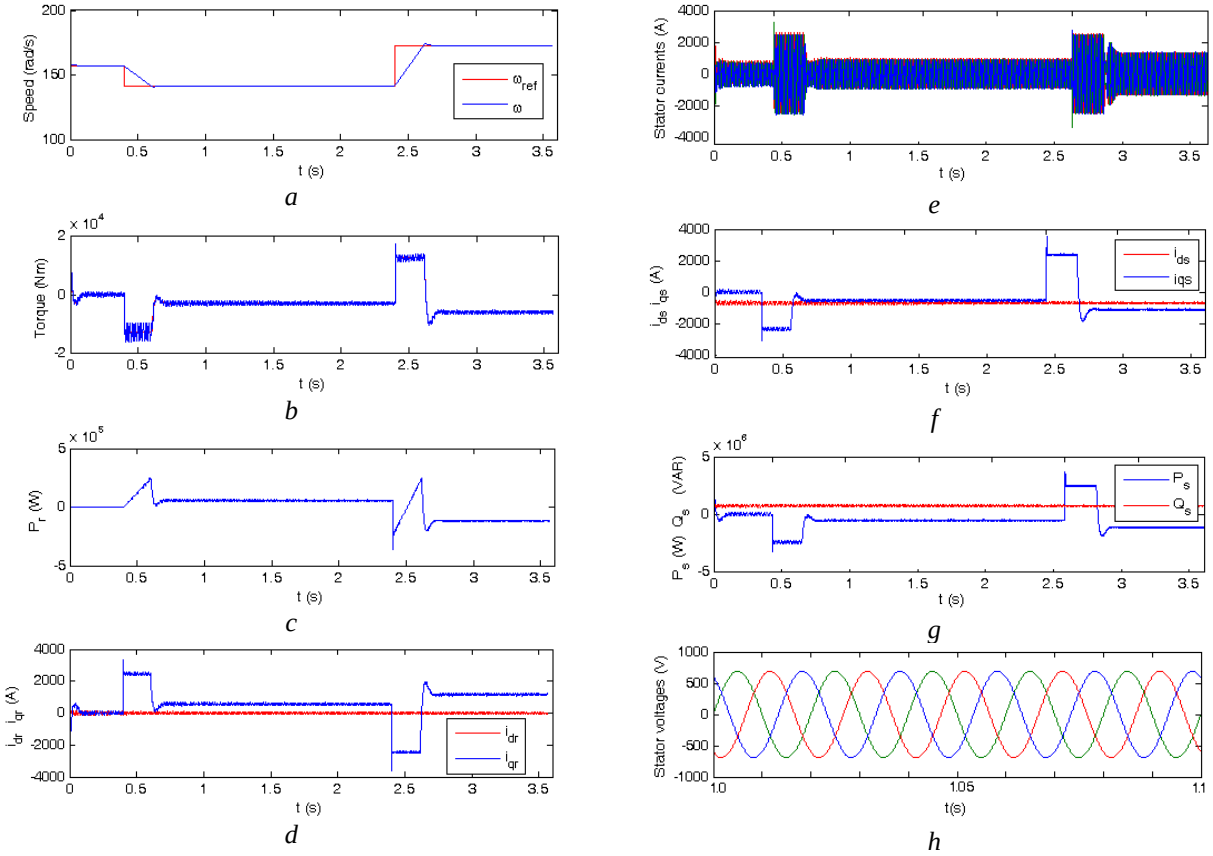

Figure 10. *Simulation results a) Wind speed, b) Torque, c) Active power of rotor, d) i_{dr} and i_{qr} currents, e) Stator phase currents, f) i_{ds} and i_{qs} currents, g) P_s and Q_s powers h) Stator phase voltages*

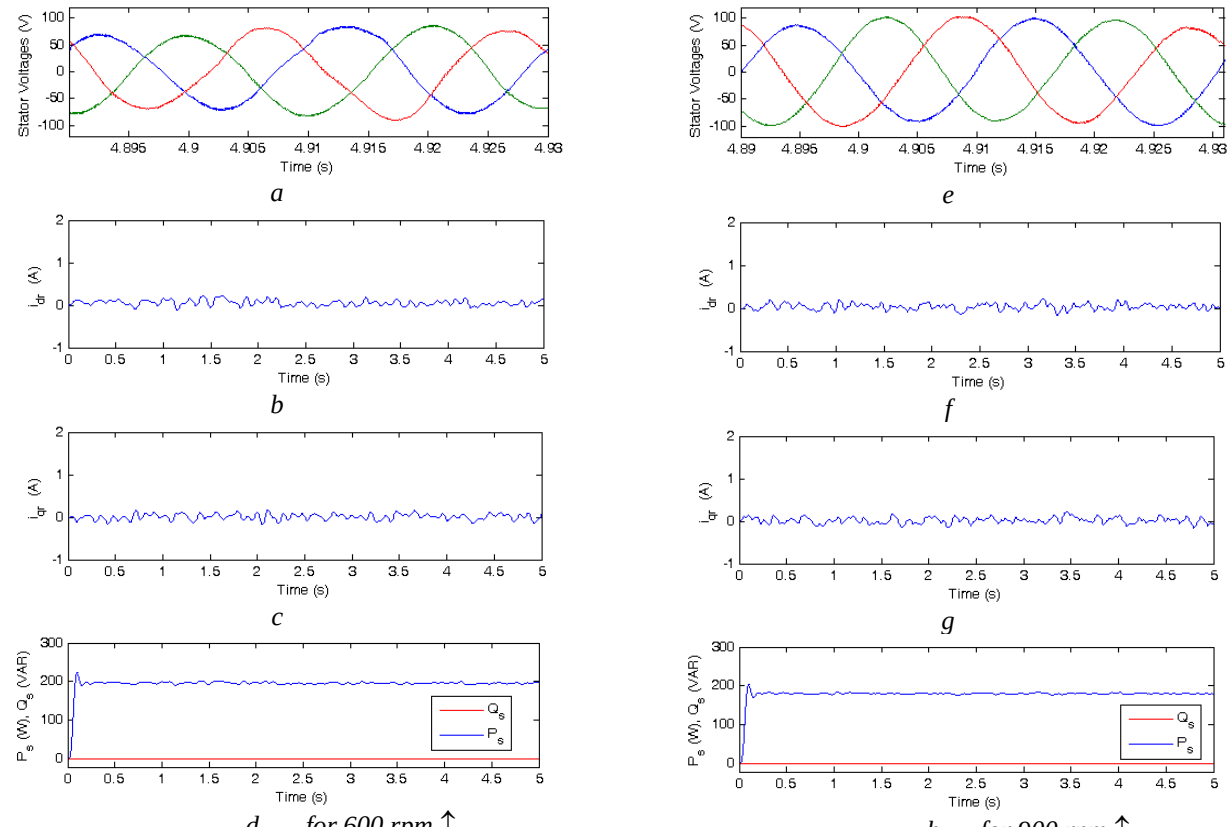

Figure 11. *Experimental results a) Stator phase voltages, b) i_{dr} and c) i_{qr} currents, d) P_s and Q_s powers for 600 rpm and, e) Stator phase voltages, f) i_{dr} and, g) i_{qr} currents, h) P_s and Q_s powers for 900 rpm*

Table 2. *Parameters of the DFIG used in simulation*

Parameter	Value	Unit
Stator frequency (f_s)	50	Hz
Nominal stator power (P_s)	2	MW
Nominal stator voltage (V_s)	690	V
Nominal stator current (I_s)	1760	A
Number of pole pairs (p)	2	
Maximum slip (s_{max})	1/3	
Nominal torque (T_{em})	12732	Nm
Synchronous speed (n_s)	1500	d/dk
Stator one-phase winding resistance(R_s)	2.6	mΩ
Rotor one-phase winding resistance (R_r)	2.9	mΩ
Magnetization inductance (L_m)	2.5	mH
Stator leakage inductance ($L_{s\sigma}$)	0.087	mH
Rotor leakage inductance ($L_{r\sigma}$)	0.087	mH
Conversion rate (N_s/ N_r)	4	
Inertia (J)	127	Kgm^2
Friction coefficient (B)	0.001	Kgm^2/s
Switching frequency (f_{sw})	4000	(Hz)
Switching period time (T_s)	$1/f_{sw}$	s

Table 3. *Parameters of the DFIG used in experimental*

Parameter	Value	Unit
Rated power (P_n)	350	W
Nominal voltage (V_n)	220	V
Nominal current (I_n)	1.4	A
Nominal speed (n_n)	1440	rpm
Mutual inductance (L_m)	942	mH
Rotor phase leakage inductance ($L_{\sigma r}$)	89	mH
Stator phase leakage inductance ($L_{\sigma s}$)	89	mH
Stator phase leakage resistance (R_1)	28.25	Ω
Rotor phase leakage resistance (R_2)	3.93	Ω

When the generator rotor speed changed during experiments, amplitude and frequency of the stator voltage remained stable.

5. RESULTS

In this paper, a DFIG driven wind turbine system was controlled in wind speed variation and stability of voltage and frequency was ensured. The model of a 2 MW DFIG driven wind turbine system was simulated on a computer. The amplitude and frequency of the voltage generated by a DFIG were controlled at synchronous, sub-synchronous and up-synchronous operating speeds. Stability of the voltage was ensured at variable speeds and different load values using robust vector control of RSC. In the experimental study, a 350 W DFIG-based wind turbine system was set up in a laboratory. The amplitude and frequency of the voltage generated by DFIG were controlled with the DS1103 board at speeds such as 600 rpm and 900 rpm. It was experimentally measured that DFIG was not affected by speed variation and generated voltages at desired amplitude and frequency values.

CONFLICTS OF INTEREST

No conflict of interest was declared by the authors.

REFERENCES

[1] Nair, A. R., Bhattarai, R., Smith, M., and Kamalasadan, S., "Parametrically robust identification based sensorless control approach for doubly fed induction generator", IEEE Transactions on Industry Applications, 57 (1): 1024-1034, (2021).

[2] Jerin, A.R.A., Kaliannan, P., Subramaniam, U., Moursi, M.S.E., "Review on FRT solutions for improving transient stability in DFIG-WTs", IET Renewable Power Generation, 12(15): 1786-1799, (2018).

[3] Hu, J., Li, Y., Zhu, J., "Multi-objective model predictive control of doubly-fed induction generators for wind energy conversion", IET Generation, Transmission & Distribution, 13(1): 21-29, (2019).

[4] Karakasis, N., Tsioumas, E., Jabbour, N., Bazzi, A.M., Mademlis, C., "Optimal efficiency control in a wind system with doubly fed induction generator", IEEE Transactions on Power Electronics, 34(1): 356-368, (2019).

[5] Ouyang, J., Tang, T., Diao, Y., Li, M., Yao, J., "Control method of doubly fed wind turbine for wind speed variation based on dynamic constraints of reactive power", IET IET Renewable Power Generation, 12(9): 973-980, (2018).

[6] Chau, T.K., Yu, S.S., Fernando, T.L., Lu, H.H.C., Small, M., "A novel control strategy of DFIG wind turbines in complex power systems for enhancement of primary frequency response and LFOD", IEEE Transactions on Power Systems, 33(2): 1811-1823, (2018).

[7] Bhattarai, R., Gurung, N., Thakallapelli, A., Kamalasadan, S., "Reduced-order state observer-based feedback control methodologies for doubly fed induction machine", IEEE Transactions on Industry Applications, 54(3): 2845-2856, (2018).

[8] Abo-Khalil, A.G., Alghamdi, A., Tlili, I., Eltamaly, A.M., "Current controller design for DFIG-based wind turbines using state feedback control", IET Renewable Power Generation, 13(11):1938-1948, (2019).

[9] Moreira, A.B., Dos Santos Barros, T.A., Teixeira, V.S.C., Souza, R.R., Paula, M.V., Filho, E.R., "Control of powers for wind power generation and grid current harmonics filtering from doubly fed induction generator: Comparison of two strategies", IEEE Access, 7: 32703-32713, (2019).

[10] Hu, Y.L., Wu, Y.K., "Approximation to frequency control capability of a DFIG-based wind farm using a simple linear gain droop control", IEEE Transactions on Industry Applications, 55(3): 2300-2309, (2019).

[11] Cai, L.J., Erlich, I., "Doubly fed induction generator controller design for the stable operation in weak grids", IEEE Transactions on Sustainable Energy, 6(3): 1078-1084, (2015).

[12] Wu, C., Nian, H., "Stator harmonic currents suppression for DFIG based on feed-forward regulator under distorted grid voltage", IEEE Transactions on Power Electronics, 33(2): 1211-1224, (2018).

[13] Kashkooli, M.R.A., Madani, S.M., Lipo, T.A., "Improved direct torque control for a DFIG under symmetrical voltage dip with transient flux damping", IEEE Transactions on Industrial Electronics, 67(1): 28-37, (2020).

[14] Tiwari, S.K., Singh, B., Goel, P.K., "Design and control of autonomous wind–solar system with DFIG feeding 3-phase 4-wire loads", IEEE Transactions on Industry Applications, 54 (2): 1119-1127, (2018).

[15] Tiwari, S.K., Singh, B., Goel, P.K., "Control of wind–diesel hybrid system with BESS for optimal operation", IEEE Transactions on Industry Applications, 55(2): 1863-1872, (2019).

[16] Song, Y., Blaabjerg, F., "Analysis of middle frequency resonance in DFIG system considering phase-locked loop", IEEE Transactions on Power Electronics, 33(1): 343-356, (2018).

[17] Sarma, N., Tuohy, P.M., Apsley, J.M., Wang, Y., Dijurovic, S., "DFIG stator flux-oriented control scheme execution for test facilities utilising commercial converters", IET Renewable Power Generation, 12(12): 1366-1374, (2018).

[18] Shao, H., Cai, X., Li, Z., Zhou, D., Sun, S., Guo, L., Cao, Y., and Rao, F., "Stability enhancement and direct speed control of DFIG inertia emulation control strategy", IEEE Access, 7: 120089-120105, (2019).

[19] Li, L., Nian, H., Ding, L., Zhou, B., "Direct power control of DFIG system without phase-locked loop under unbalanced and harmonically distorted voltage", IEEE Transactions on Energy Conversion, 33 (1): 395-404, (2018).

[20] Zhou, D., Zhang, G., Blaabjegr, F., "Optimal selection of power converter in DFIG wind turbine with enhanced system-level reliability", IEEE Transactions on Industry Applications, 54(4): 3637-3644, (2018).

[21] Kou, P., Liang, D., Li, J., Gao, L., Ze, Q., "Finite-control-set model predictive control for DFIG wind turbine", IEEE Transactions on Automation Science and Engineering, 15(3):1004-1013, (2018).

[22] Cruz, S.M.A., Marques, G.D., Gonçalves, P.F.C., Iacchetti, M.F., "Predictive torque and rotor flux control of a DFIG-DC system for torque ripple compensation and loss minimization", IEEE Transactions on Industrial Electronics, 65(12): 9301-9310, (2018).

[23] Yang, J., Tang, W., Zhang, G., Sun, Y., Ademi, S., Blaabjerg, F., "Sensorless control of brushless doubly fed induction machine using a control winding current MRAS observer", IEEE Transactions on Industrial Electronics, 66(1): 728-738, (2019).

[24] Subudhi, B., Ogeti, P.S., "Optimal preview stator voltage-oriented control of DFIG WECS", IET Generation, Transmission & Distribution, 12(4): 1004-1013, (2018).

[25] Moradi, H., Alinejad-Beromi, Y., Yaghobi, H., "Bustan D. Sliding mode type-2 neuro-fuzzy power control of grid-connected DFIG for wind energy conversion system", IET Renewable Power Generation, 13(13): 2435-2442, (2019).

[26] Djilali, L., Sanchez, E.N., Belkheiri, M., "Real-time neural sliding mode field oriented control for a DFIG-based wind turbine under balanced and unbalanced grid conditions", IET Renewable Power Generation, 13(4): 618-632, (2019).